

# Milliscale Substrate Curvature Promotes Myoblast Self-Organization and Differentiation

Che J. Connon\* and Ricardo M. Gouveia\*

Biological tissues comprise complex structural environments known to influence cell behavior via multiple interdependent sensing and transduction mechanisms. Yet, and despite the predominantly nonplanar geometry of these environments, the impact of tissue-size (milliscale) curvature on cell behavior is largely overlooked or underestimated. This study explores how concave, hemicylinder-shaped surfaces 3–50 mm in diameter affect the migration, proliferation, orientation, and differentiation of C2C12 myoblasts. Notably, these milliscale cues significantly affect cell responses compared with planar substrates, with myoblasts grown on surfaces 7.5–15 mm in diameter showing prevalent migration and alignment parallel to the curvature axis. Moreover, surfaces within this curvature range promote myoblast differentiation and the formation of denser, more compact tissues comprising highly oriented multinucleated myotubes. Based on the similarity of effects, it is further proposed that myoblast susceptibility to substrate curvature depends on mechanotransduction signaling. This model thus supports the notion that cellular responses to substrate curvature and compliance share the same molecular pathways and that control of cell behavior can be achieved via modulation of either individual parameter or in combination. This correlation is relevant for elucidating how muscle tissue forms and heals, as well as for designing better biomaterials and more appropriate cell–surface interfaces.

## 1. Introduction

Skeletal muscle tissues are comprised of highly aligned, multinucleated muscle fibers arising from the fusion of mononucleated myoblasts. In mammals, early muscle development involves the fusion of primary myoblasts to form myotubes,

which subsequently serve as scaffolds for the oriented fusion and maturation of secondary myoblasts and the formation of muscle fibers.<sup>[1]</sup> The alignment and fusion of myoblasts is essential for the maintenance of muscle structural and contractile function; however, the factors directing primary myotube orientation are still poorly understood.<sup>[2]</sup> Possible cues include structural, biochemical, and mechanical factors affecting cell adhesion, motility, orientation, and polarization.<sup>[3]</sup> Many of these cues have been explored for their potential to produce structured skeletal muscle tissues with clinical and biomedical applications (i.e., reproducing their native-like structure to better replace muscle function lost to injury or disease).<sup>[4]</sup> More recently, muscle tissue engineering has also been applied to the generation of alternative food source (i.e., animal cultured meat).<sup>[5]</sup>

Previous attempts to (re)create structured skeletal muscle tissues, either in 2D or 3D, have relied mostly on the use of micro- and nanopatterned surfaces.<sup>[6]</sup> In particular, early tissue engineering approaches have been focused on exposing

skeletal or cardiac muscle cell cultures to a wide range of surface interfaces presenting multiple parallel nano- or microtopographic features capable of directing the alignment of individual cells.<sup>[7]</sup> However, these methods depend on the relatively complex surface fabrication technologies and allow only the production of cell sheets monolayers. More recent efforts have used cyclic force<sup>[8]</sup> or uniaxially patterned scaffolds produced by electrospinning,<sup>[9]</sup> extrusion,<sup>[10]</sup> and freeze-drying approaches<sup>[11]</sup> as methods to induce muscle cell organization in 3D, but even in these cases cell spreading and alignment were still restricted by material biocompatibility and porosity. As such, engineering 3D muscle tissues with aligned structures remains a challenging endeavor.

The capacity of nano- and microtopographical cues to affect cell alignment and phenotype is in part dependent on their similarity to components of the extracellular matrix, particularly of its fibrillar elements,<sup>[12]</sup> as well as on the scale of the cellular surface-sensing, surface-adhesive machinery.<sup>[13]</sup> In contrast, less is known about the possible impact of tissue-scale (i.e., milliscale) topographies on cellular behavior. This aspect of cellular response to the surrounding environment has to date been largely overlooked,<sup>[14]</sup> possibly owing to methodological difficulties. However, being the prevalent geometry in biological tissues, it is reasonable to assume that milliscale surface curvature

Prof. C. J. Connon  
Tissue Engineering Lab Biosciences Institute  
Newcastle University, International Centre for Life  
Newcastle upon Tyne NE1 3BZ, UK  
E-mail: che.connon@newcastle.ac.uk

Dr. R. M. Gouveia  
Biosciences Institute  
Newcastle University, International Centre for Life  
Newcastle upon Tyne NE1 3BZ, UK  
E-mail: ricardo.gouveia@newcastle.ac.uk

 The ORCID identification number(s) for the author(s) of this article can be found under <https://doi.org/10.1002/adbi.202000280>.

© 2021 The Authors. Advanced Biology published by Wiley-VCH GmbH. This is an open access article under the terms of the Creative Commons Attribution License, which permits use, distribution and reproduction in any medium, provided the original work is properly cited.

DOI: 10.1002/adbi.202000280

may be a fundamental factor regulating cell migration, proliferation, and fate.<sup>[15]</sup> Indeed, this notion has increasingly been gaining support from the observation that cells, either individually or as a population, are able to respond to surface curvature cues far bigger than the size of the cells themselves.<sup>[16]</sup> Recent studies have even indicated that cell contact guidance induced by nanopography can be overruled by milliscale and mesoscale surfaces with various geometries (e.g., concave and convex cylinders and spheres, saddles, torus).<sup>[17]</sup> Appropriately, milliscale surface curvature has already been proved a very simple and effective cue for directing cells to align for tissue engineering purposes. For example, dome-shaped, convex substrate cues in the millimeter range have recently been used to generate corneal tissue equivalents with improved characteristics, i.e., tissues with native-like structure and function that do not rely on scaffolds or carriers.<sup>[18]</sup> Conversely, concave curvature should play a predominant role during organogenesis, with embryonic tissues such as myotomes and dermomyotomes (from which skeletal muscles derive) displaying such geometry.

To understand the role of milliscale surface curvature on muscle cell alignment, and its feasibility as a cue to engineer structured muscle tissues, we thus used hemicylinder-shaped concave surfaces with 3–50 mm curvature diameter and analyzed the results in terms of impact on cell adhesion and proliferation, migration, orientation, and differentiation. We

showed that the same substrate curvature leading to myoblast alignment over large-scale areas also promoted cell differentiation. Together, our findings provide new insights into the mechanism of myotube organization in response to geometry cues while creating a novel and easier system to guide skeletal muscle cell alignment and engineering structured muscle tissues with long-range myotube orientation via bottom-up fabrication methods.

## 2. Results

### 2.1. Curved Cell Culture Templates Created from Glass Tubes Have Smooth Surfaces

To test the effect of curved surface templates on muscle cell growth, customized half-pipe glass tubes 3–50 mm in diameter were manufactured and subsequently treated with a cell-adhesive peptide coating on their concave side (Figure 1a,b). The diameter range of these tubes aimed at defining an optimized myoblast response to milliscale surface curvature, as informed by previous studies,<sup>[17a–c,19]</sup> whereas their concave geometry potentiated their use as stand-alone culture chambers (Figure 1a). Flat glass coverslips were similarly coated and used as planar geometry controls (Figure 1a). All surfaces were

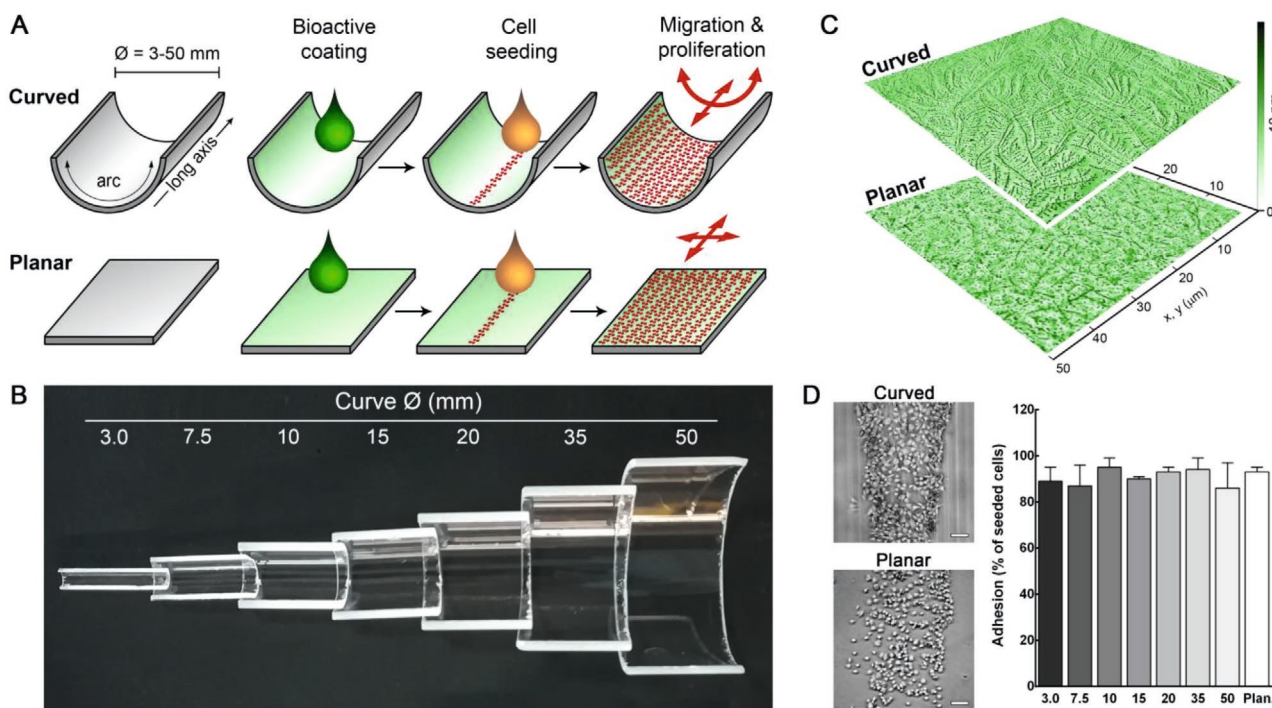


**Figure 1.** Development of milliscale curved surface templates for skeletal muscle cell culture. A) Schematic representation of culture setup to evaluate the effect of milliscale surface curvature on myoblast behavior. Curved, hemicylinder-shaped surfaces with diameter ( $\varnothing$ ) ranging between 3 and 50 mm coated with cell-adhesive bioactive PA were seeded with C2C12 myoblasts in a line running along the surfaces' long axis, for subsequent evaluation of impact of curvature on cell migration, proliferation, orientation, and tissue growth. Coated glass coverslips were used as planar control surfaces. B) Top-view photograph of custom-made glass hemicylinder surfaces post-coated. C) Nanopography of curved and planar analyzed by atomic force microscopy. Images showed that the bioactive coating on both types of surfaces was continuous, uninterrupted, and comprised by cell-adhesive PA fibrils distributed uniformly and creating a fairly smooth surface (roughness lower than 10 nm). D) Most of C2C12 myoblasts adhered to coated surfaces within 1 h independently of template curvature (right panel), forming a 500  $\mu\text{m}$ -wide line spanning the templates' long axis as shown by representative microscopy images (left panel). Values correspond to average  $\pm$  s.d. from six independent experiments ( $n = 6$ ). Scale bars, 100  $\mu\text{m}$ .

shown to present stable, uniformly distributed peptide coating, as observed by phase-contrast and fluorescence microscopy (Figure S1, Supporting Information). To verify that both curved and planar surfaces did not present meaningful microtopographical features capable of influencing cell behavior (e.g., alignment-inducing grooves, pits, or indentations), template topography was analyzed by atomic force microscopy (AFM) (Figure 1c). Results showed that all curved and planar templates were indistinguishable at the nano-level and comprised smooth coated templates formed by regular and continuous deposits of bioactive peptide nanotapes averaging  $7 \pm 4$  nm in roughness but without larger microtopographical structures capable of inducing cell anisotropy (Figure 1c).

## 2.2. Myoblasts Are Able to Adhere and Grow on Curved Surface Templates

C2C12 myoblasts were subsequently grown on both curved and planar surface templates, using a mask to seed cells in a 500  $\mu\text{m}$ -wide line spanning the template's long axis. This method allowed to better define the cells' initial position and facilitate monitoring their subsequent migration, as well as

their proliferation and preferred orientation during the first 3 d in culture (Figure 1a). All templates were able to promote myoblast adhesion within 1 h of seeding, irrespective of surface curvature (Figure 1d, left panels); moreover, the number of attached cells was similar between the different templates after 24 h and corresponded to 86% or more of the initial seeding (Figure 1d, graph). But most importantly, despite the high density of the seeding, cells did not clump together and remained separated during the initial 3 d in culture, allowing individual cell tracking.

## 2.3. Substrate Curvature Induces Faster Myoblast Migration and Anisotropic Cell Distribution

The impact of surface curvature on cell migration and proliferation was evaluated in subconfluent cultures for 3 d after initial cell seeding (Figure 2) to better track individual cells and avoid arrested growth from contact inhibition. Cell doubling time quantified at Day 3 of culture showed to be increased with reduced curvature diameter, albeit not to a significant level (Figure 2a). In contrast, curvature was shown to impact myoblast migration rate, with individual cells showing significantly

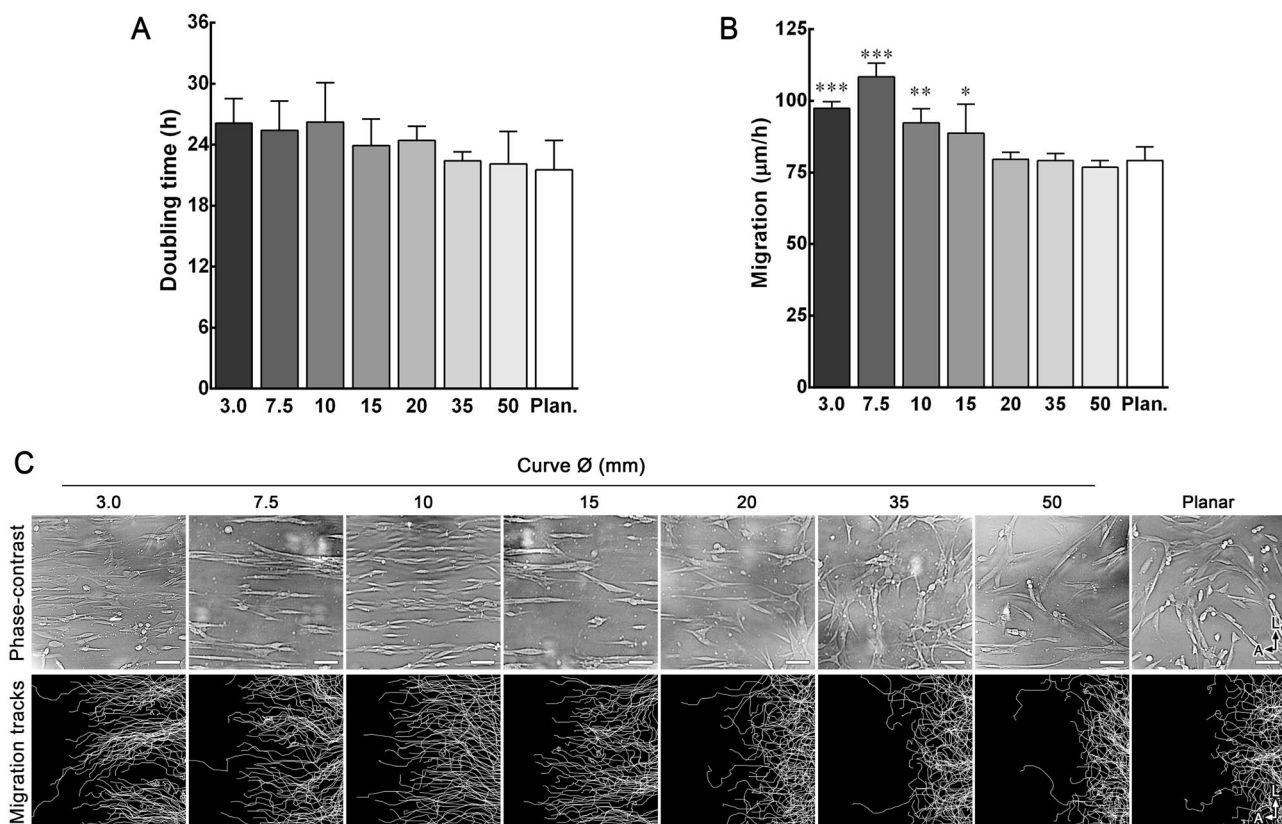


**Figure 2.** Effect of milliscale curved surface templates on myoblast proliferation and migration. A) Initial proliferation of C2C12 myoblasts on curved and planar surfaces, quantified as doubling time. B) Myoblast migration, quantified from movement of individual cells. Values correspond to average  $\pm$  s.d. from six independent experiments ( $n = 6$ ) obtained over the first 3 d postseeding (\*, \*\*, and \*\*\* corresponded to  $p < 0.05$ , 0.01, and 0.001, respectively). C) Orientation of C2C12 cells at the front of migration. The distribution and migration (bottom panel) of myoblasts growing on curved and planar surfaces was imaged 3 d after seeding using time-lapse, phase-contrast microscopy, and evaluated relatively to the main geometrical orientations ( $a =$  arc axis,  $l =$  long axis). Representative cell distribution microscopy images from three independent fields of view (top panel) and migration tracks calculated for 100 individual myoblasts (bottom panel) are shown. Scale bars, 100  $\mu\text{m}$ .

faster migration rates when grown on surfaces with smaller curvature diameters (Figure 2b). This corresponded to an increase from  $79 \pm 5 \mu\text{m h}^{-1}$  on planar to  $89 \pm 10 \mu\text{m h}^{-1}$  on curved surfaces with  $\varnothing = 15 \text{ mm}$ , up to  $108 \pm 5 \mu\text{m h}^{-1}$  on  $\varnothing = 7.5 \text{ mm}$  (Figure 2b). Moreover, myoblasts grown on curved surfaces migrated outward from their original seeding site showing distinctly polarized morphologies while following very consistent migration tracks (Figure 2c). Specifically, individual C2C12 cells growing on concave surfaces 3–15 mm in diameter showed well-organized, anisotropic distribution, fusiform morphologies (Figure 2c, top panel) and migrated in preponderantly linear pathways along the arc of curvature (Figure 2c, bottom panel). Conversely, myoblasts on less curved ( $\varnothing = 20\text{--}50 \text{ mm}$ ) or planar surfaces showed isotropic distributions, with shorter, nonlinear migration tracks (Figure 2c). Together, this indicated that, even at the milliscale range, concave surface curvature affected C2C12 cell migration and organization.

#### 2.4. Substrate Curvature Promotes Higher Density of Viable Myoblasts

Interestingly, curved surface templates were also shown to impact the total density of myoblasts upon confluence (i.e., after 5-d culture in proliferation medium; Figure 3). Specifically, the

density of C2C12 cells growing on curved surfaces was higher than that on planar surfaces (Figure 3), with 75 and 10 mm  $\varnothing$  templates showing to support increased cell numbers significantly ( $152 \pm 19\%$  and  $133 \pm 13\%$  of planar controls, respectively; Figure 3b). This effect was not derived from differences in cell viability, as this was kept equally high (90% or above) in all culture templates analyzed (Figure 3a,c).

#### 2.5. Substrate Curvature Induces Myoblast Alignment

Most importantly, myoblasts grown on curved surface templates were shown to self-organize in very specific orientations. In particular, cells grown on curved surfaces within the 7.5–20 mm  $\varnothing$  range migrated from the initial seeding line up toward the edge of the template assuming a predominant orientation parallel to the arc of curvature. This cell alignment also corresponded to a preferential nuclei orientation along the arc of curvature and was kept throughout the proliferation period of culture (Figure 3a). The effect of surface curvature on myoblast alignment was also quantified at Day 5 by analyzing the coherent position of cells imaged by phase-contrast microscopy, with orientation assigned in  $1^\circ$  bins within a  $180^\circ$  range, and where  $0/180^\circ$  and  $90^\circ$  corresponded to the long axis and the arc of curvature, respectively (Figure 4). The frequency

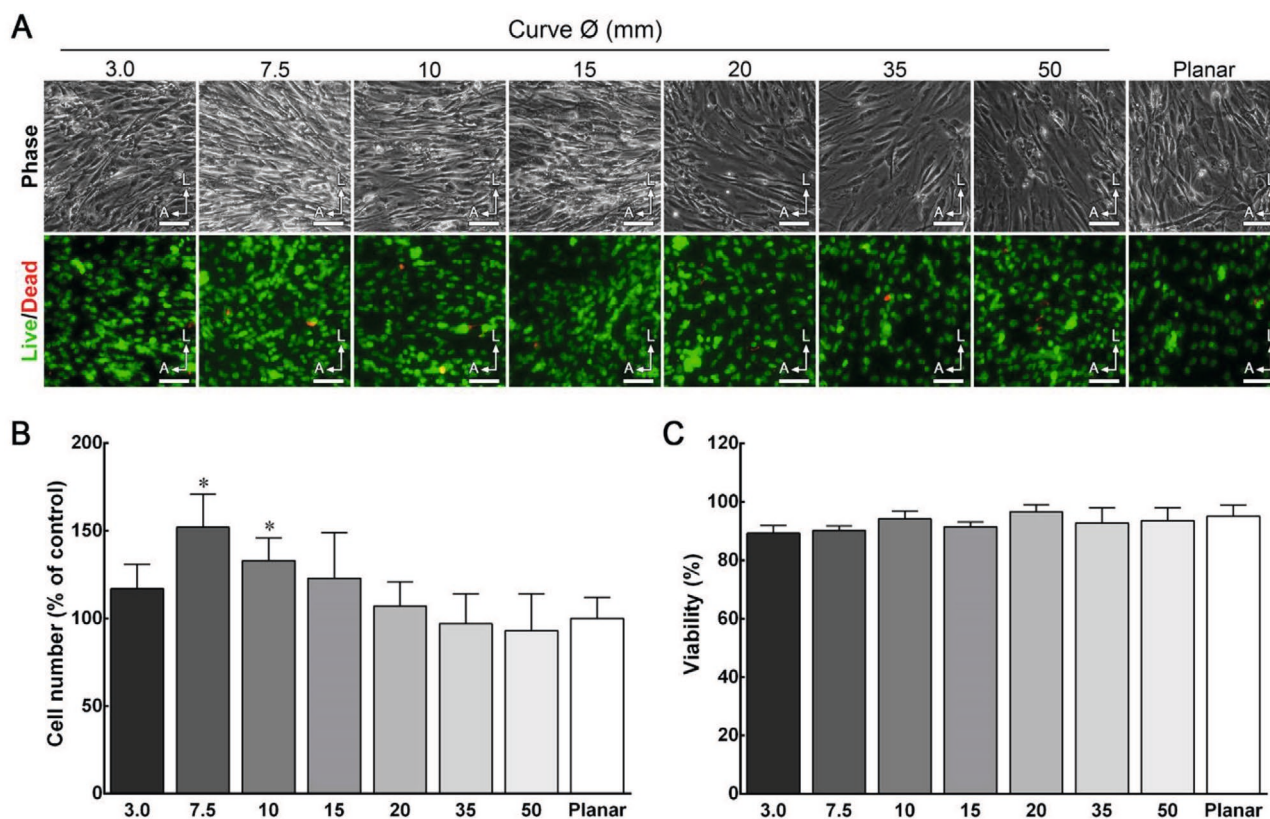


**Figure 3.** Effect of milliscale curved surface templates on myoblast density and viability upon confluence. A) Representative microscopy of C2C12 cells grown for 5 d on curved and planar surfaces with defined orientations ( $a$  = arc axis,  $l$  = long axis). Cultures were analyzed for their density by phase-contrast microscopy (top panel) and viability following Live (green)-Dead (red) double stain fluorescence microscopy (bottom panel). Scale bars, 100  $\mu\text{m}$ . B) Total number of live cells using the Alamar Blue assay, and C) cell viability was calculated from the average  $\pm$  s.d. of six independent experiments ( $n = 6$ ; \* corresponded to  $p < 0.05$ ).

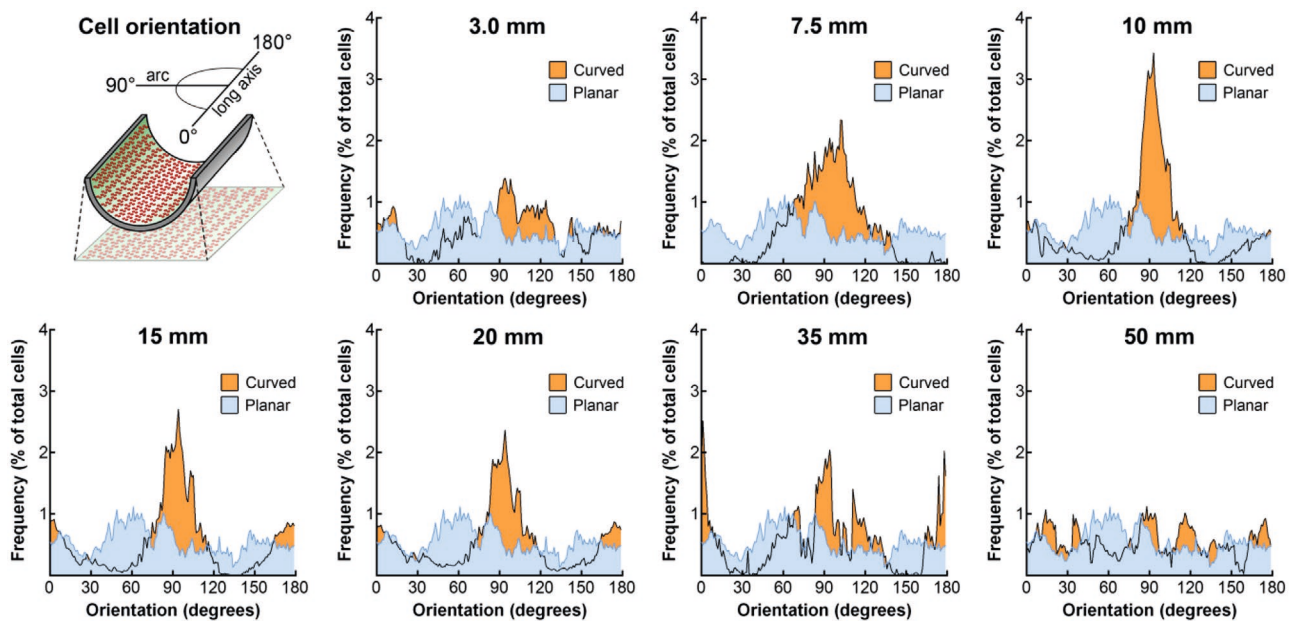


**Figure 4.** Effect of milliscale curved surface templates on myoblast alignment. A) The orientation of individual C2C12 cells on curved and planar surfaces was analyzed from phase-contrast microscopy images after 5 d in culture, and orientation vectors quantified, grouped in  $1^\circ$  bins, and represented as average frequency distribution within a  $0^\circ$ – $180^\circ$  range, with  $0^\circ/180^\circ$  and  $90^\circ$  corresponding to the long and arc axis, respectively (top left schematic). Cell orientation on curved surfaces of different diameter (orange) was compared to that on planar surfaces (blue) in six independent experiments ( $n = 6$ ).

distribution of myoblasts grown to confluence on curved surfaces with  $\varnothing = 7.5, 10, 15,$  and  $20$  mm showed clearly defined peaks around the  $90^\circ$  axis (Figure 4), which corresponded well with the predominantly oriented migration observed previously along the arc of curvature. Such prevalent distribution was absent on surface templates with higher or lower curvatures, including on planar surface templates (Figure 4, blue lines). Curved templates with  $\varnothing = 10$  and  $15$  mm showed the highest frequency of aligned cells (54% and 37% frequency distribution in the  $90 \pm 10^\circ$  range, respectively). In contrast, planar templates showed the lowest cell alignment, with only 13% of myoblasts oriented within the  $90 \pm 10^\circ$  range, a frequency value close to absolute random distribution (11%).

Altogether, these results demonstrated that C2C12 myoblasts are capable of sensing milliscale curvature, namely, in the  $7.5$ – $15$  mm  $\varnothing$  range, and responded to such cues by migrating faster and achieving a denser, highly aligned organization.

## 2.6. Substrate Curvature Promotes Myoblast Differentiation

Finally, the impact of milliscale substrate curvature on myoblast differentiation was investigated at the molecular level. Cells on curved and planar surfaces were further grown in differentiation medium for an additional 5 d period and subsequently analyzed for the expression of myoblast and myogenic markers<sup>[2a,20]</sup> by reverse-transcription quantitative polymerase chain reaction (RT-qPCR) (Figure 5). Cells grown on curved surface templates showed consistent trends characterized by reduced expression of undifferentiated cell markers *Pax7* (Figure 5a) and increased expression of early- and late-stage differentiation markers (Figure 5b,c, respectively). Specifically,

cells on curved templates with  $\varnothing = 3$ – $10$  mm showed significantly lower *Pax7* levels compared to those on planar controls (Figure 5a). A similar inhibitory trend was observed for *Abcg2*, albeit with smaller, not significant differences (Figure 5a). In contrast, cells grown on curved templates with  $\varnothing = 3$ – $15$  mm showed significantly higher transcription of genes coding for the Myoblast Determination Protein 1 (*Myod1*; Figure 5b) and for Myosin Heavy Chain 3 and myogenin (*Myh3* and *Myog*, respectively; Figure 5c), all important factors in skeletal muscle differentiation.<sup>[2a]</sup> However, the expression of the gene coding for acetylcholinesterase *Ache*, an essential factor of the neuromuscular junction,<sup>[21]</sup> was not affected by surface template curvature (Figure 5b).

Finally, differentiated muscle cell cultures grown on the various templates for a total of 10 d were imaged by phase-contrast and immunofluorescence microscopy (Figure 6). After the 5-d differentiation period, cells on both curved and planar templates were highly dense and cultures became stratified, with a second layer of cells growing over the confluent bottom monolayer (Figure 6a, phase-contrast). A considerable number of these cells assumed a longer, tubular morphology (average length and width of  $334 \pm 128$  and  $28 \pm 9 \mu\text{m}$ , respectively) and became multinucleated (Figure 6a). These features were consistent with the process of skeletal muscle cell differentiation, which involves myocyte fusion and formation of long myotubes, and were particularly evident on curved templates with  $\varnothing = 3$ – $20$  mm.

Moreover, the expression of myogenic markers at the protein level (via analysis of signal intensity from micrographs) was consistent with the RT-qPCR data. Overall, cells grown on curved surface templates showed increased expression of Myosin Heavy Chain 3 (MYH) and myogenin (MYOD)

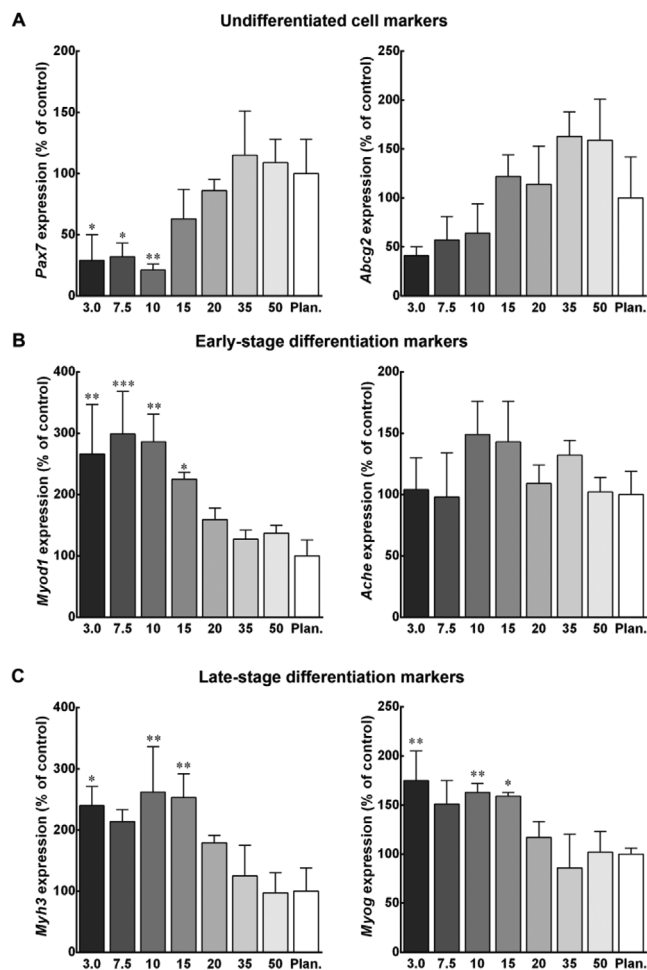


**Figure 5.** Effect of milliscale curved surface templates on the expression of myogenic markers at the transcriptional level. C2C12 cells grown on curved and planar surfaces for 10 d were analyzed for their expression of A) undifferentiated myoblast markers *Pax7* and *Abcg2*, B) early-stage differentiation markers *Myod1* and *Ache*, and C) late-stage differentiation markers *Myh3* and *Myog* by RT-qPCR, normalized for *Gapdh* house-keeping gene expression. Average  $\pm$  s.d. of four independent experiments ( $n = 4$ ) were represented as percentage of control (\*, \*\*, and \*\*\* corresponded to  $p < 0.05$ ,  $0.01$ , and  $0.001$ , respectively).

differentiation markers, as well as reduced PAX7 expression (Figure 6). MYH expression in particular was significantly increased on curved templates with  $\varnothing = 10$  mm, whereas cells on templates with  $\varnothing = 3$  and  $7.5$  mm showed significant higher MYOD and lower PAX7 expression than those on planar surfaces (Figure 6b).

Interestingly, differentiated muscle cells on curved templates, namely, those with  $\varnothing = 10$ – $15$  mm, consistently showed a prevalent alignment along the arc of curvature (Figure 6a and Figure S2, Supporting Information), thus maintaining their organized, precell fusion distribution observed at Day 5 (Figures 3 and 4). Conversely, differentiated muscle cells on planar templates failed to show any substantial increase in organization (Figure S2, Supporting Information). Together, these results indicated that a milliscale curvature of around 10 mm in  $\varnothing$  represents the optimal surface template cue for promoting

myogenesis in differentiated C2C12 cells as well as the formation of highly aligned myotubes.

### 3. Discussion

Most if not all biological soft tissues exhibit some degree of anisotropy, which in turn influences their structural and mechanical properties underpinning their function.<sup>[2a,22]</sup> Tissue anisotropy not only has implications for how cells organize themselves into collective entities in vivo but is also critical in tissue engineering. One of the main challenges in tissue engineering has been the development of simple and reliable culture systems that allow cells to recapitulate their natural organization and that of their extracellular matrix.<sup>[23]</sup> This organization is particularly crucial in engineered skeletal and cardiac muscle, where aligning myoblasts in preparation for myotube formation is essential to reproduce the native structure and generate effective vector contractile power of tissues.<sup>[4,24]</sup> In this study, we demonstrated that milliscale curvature cues reproducing tissue-sized, concave surface geometries can elicit such anisotropy in vitro. Specifically, it showed that C2C12 myoblasts were able to respond to tissue-sized surface curvature cues several orders of magnitude above that of individual cells. With the exception of 3 mm diameter surfaces, the cellular impact of the milliscale cues explored in this study increased with increased curvature. Myoblasts grown on concave, hemicylinder-shaped surfaces with a 10 mm curvature diameter were shown to migrate faster, grow into highly aligned multilayers, fuse and differentiate into myotubes in larger numbers, and ultimately achieve a higher level of self-organization compared with counterparts growing on planar surfaces.

Consequently, these results support the idea that milliscale surface curvature can be feasibly applied as a simple topographical cue for generating highly dense, structured skeletal muscle tissues in vitro. Conversely, they indicate that concave geometries in the milliscale range may play a fundamental role in muscle tissue development, maintenance, and repair. This represents a somewhat unexpected finding, as the evident muscle geometries with diameter spanning between 0.1 and 10 mm found in natural tissues (e.g., muscle fibers and fascicles) have convex shapes.<sup>[25]</sup> Such convex geometries also represent an important factor affecting cell orientation and phenotype, as recently demonstrated with cells derived from human bone marrow<sup>[17a,26]</sup> and vascular smooth muscle.<sup>[17e]</sup>

Presently, the use of cell culture surfaces with nano- and microtopographical features (grooves and channels  $1 \times 10^{-8}$ – $10^{-4}$  m wide) represents one of the most effective methods to guide cell migration and organization and create highly aligned, anisotropic muscle tissue equivalents.<sup>[6]</sup> Several studies have indeed shown that nano- and micropatterning can support the parallel alignment of myoblasts, as well as influencing their migration, fusion efficiency, and differentiation.<sup>[6]</sup> For example, surfaces exhibiting nanoscale features in the same dimension range of muscle ECM components (convex cues 100–600 nm in diameter) are able to induce myoblast alignment,<sup>[27]</sup> while parallel microgrooves 5–100  $\mu$ m wide and 1–3  $\mu$ m deep have been shown to promote myoblast differentiation and myotube alignment.<sup>[7c,27a,28]</sup> These contact guidance effects were

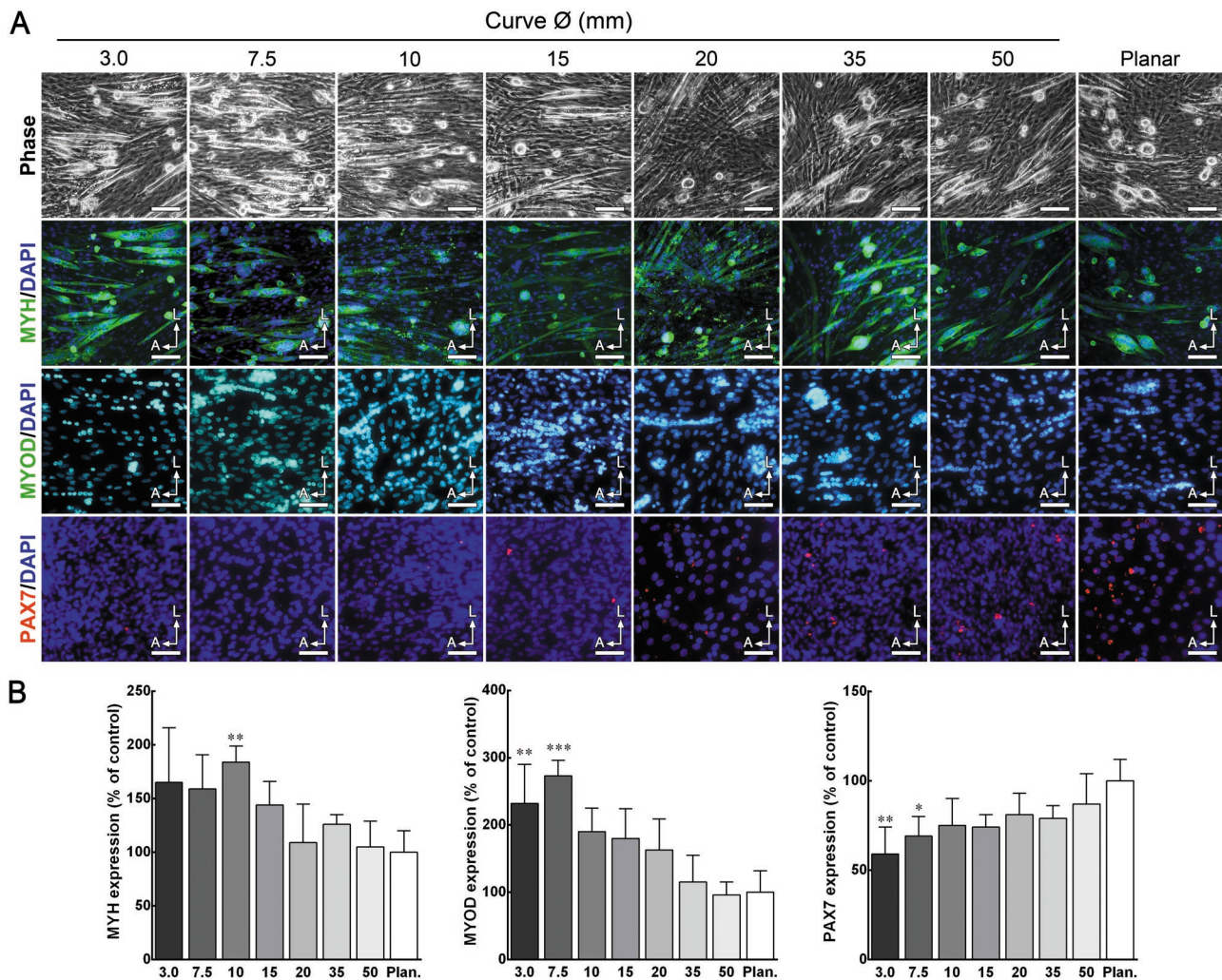


**Figure 6.** Effect of milliscale curved surface templates on the expression of myogenic markers at the protein level. A) Representative microscopy images of C2C12 cells grown for 10 d on curved and planar surfaces with defined orientations ( $a$  = arc axis,  $l$  = long axis). Cultures were analyzed for their density by phase-contrast microscopy (top panel), as well as for myoblast markers (MYH and MYOD, green; PAX7, red) (bottom panel). Cell nuclei were stained with DAPI (blue). Scale bars, 100  $\mu$ m. B) Expression of protein markers quantified as average  $\pm$  s.d. of four independent experiments ( $n = 4$ ) and represented as percentage of control (\*, \*\*, and \*\*\* corresponded to  $p < 0.05$ , 0.01, and 0.001, respectively).

independent of sharp-edge features, as shown by the use of sinusoidal-grooved microscaled patterns.<sup>[28,29]</sup>

Studies using spatial patterning to affect myogenic cells have identified several mechanisms through which cells sense and respond to nano- and microtopography. Physical contact guidance, i.e., cell alignment, has been shown to depend on the rearrangement of specific cellular components, including filopodia, focal adhesions, and intracellular stress fibers, which in turn results in changes in cell and nuclear morphology, as well as in transcription factor regulation and differential gene and protein expression via direct and/or indirect mechanotransduction pathways.<sup>[13,14]</sup> Interestingly, the impact of concave milliscale curvature cues on C2C12 myoblast behavior also seems to result from mechanosensing and mechanotransduction mechanisms (Figure 7). This hypothesis is based on the similarity between the present results and the recognized myoblast response to substrate stiffness. The role of mechanotransduction on myoblast function and

fate is well documented<sup>[12,30]</sup> and has been explored in muscle tissue engineering before.<sup>[2b,31]</sup> Specifically, surfaces reproducing the elastic modulus of muscle tissue (i.e., softer than the typical tissue culture polystyrene) were previously shown to promote myogenic differentiation<sup>[32]</sup> via mechanotransduction signaling involving the cytoplasmic inactivation of a key regulator, YAP.<sup>[33]</sup> Conversely, substrates simulating the stiffer tissue of aged muscles were shown to promote proliferative progenitor muscle cells.<sup>[34]</sup> In our proposed model, the effects of concave milliscale curvature, i.e., faster cell migration, long-range individual and collective cell alignment parallel to the arc axis, higher cell organization and tissue density, and increased myotube differentiation (Figure 7a) were because of the reduced cell-interface contacts, possibly derived from the cells' drive to minimize their free energy and optimize their packing on the available surface.<sup>[35]</sup> As predicted by both modeling<sup>[36]</sup> and in vitro studies,<sup>[26,37]</sup> when cell deformation caused by substrate curvature (pull force) partly cancels

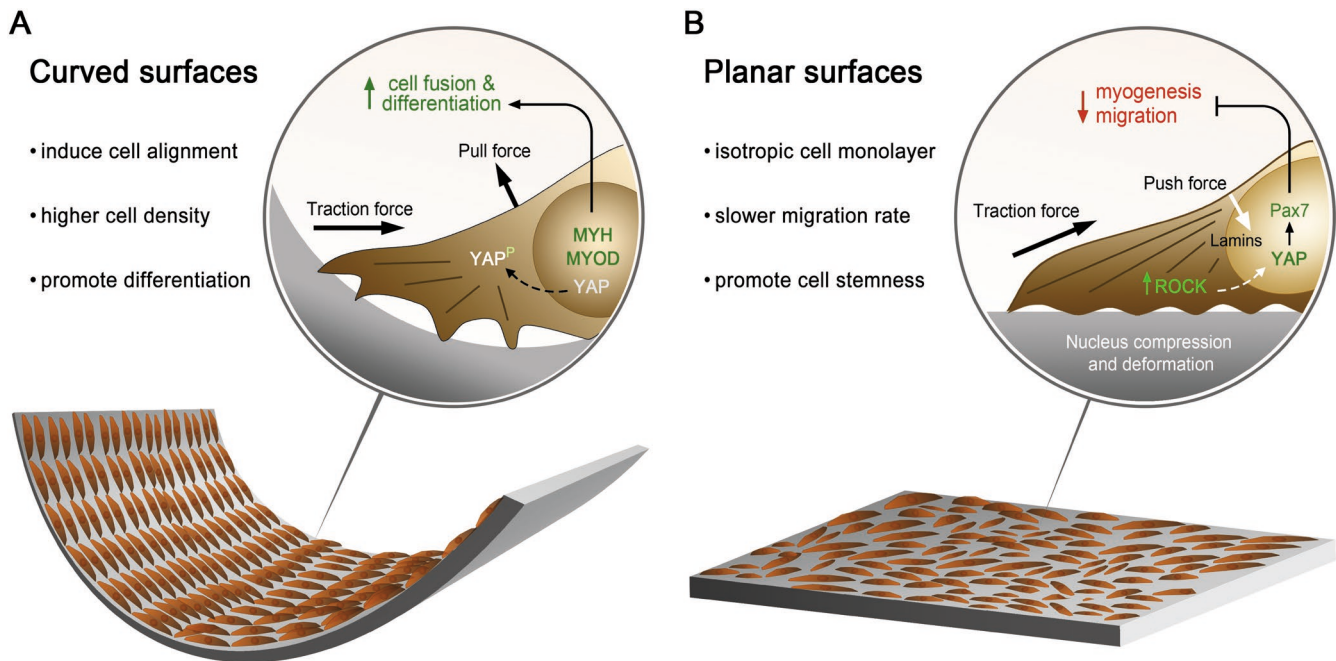


**Figure 7.** Proposed mechanism of action of milliscale curvature cues on skeletal muscle cell behavior. A) Curvature surfaces  $\approx 10$  mm  $\varnothing$  were effective in promoting myoblast alignment, with cells predominantly aligning along the arc axis, and therefore facilitating a more structured, denser accumulation of cells and enhanced myotube formation. These effects are probably derived from a balance between the traction forces inherent to the cells or cell collectives and the pull forces elicited by surface geometry. This balance is expected to minimize cell-surface contact (thus promoting migration rate) and reduce cytoskeleton and nuclear envelope tension, leading to molecular signaling similar to that from myoblasts on softer substrate environments (e.g., YAP cytoplasmic phosphorylation and inactivation, upregulation of MYH and MYOD, increased cell fusion and differentiation). B) Planar surfaces are instead expected to predominantly lead to traction-push forces promoting mechanotransduction signaling events that directly and indirectly inhibit cell migration and differentiation.

active cell contractility (intracellular traction force) then cells migrate faster and preferentially orient parallel to the curvature (arc) axis. This balance of forces subsequently leads to a cellular response involving cytoskeleton rearrangement and reduced nuclear compression typically associated with mechanoresponses to compliant substrates.<sup>[12,19c]</sup> These changes in turn lead to YAP inactivation and the consequent upregulation of myogenic factors, myoblast fusion, and myotube differentiation (Figure 7a).<sup>[30,38]</sup> These effects may depend on the high density of myoblasts obtained in our system, with close cell proximity promoting a chain of cell–cell interactions and the formation of cell collectives.<sup>[39]</sup> Together with the distribution of in-plane stresses<sup>[40]</sup> and the combined intercellular interactions, the augmented pull force exerted on such collectives over a large surface area would explain how cell behavior can be modulated by concave curvature cues orders of magnitude larger than the cells themselves. However, the oriented cell migration reported in this study during the first 3 d in culture suggests that our mechanistic model still applies at individual cell level. This interplay between forces may also explain the apparent exceptions observed from C2C12 cells grown on 3 mm  $\varnothing$  surfaces, with cell-intrinsic contractile forces becoming predominant in the more confluent, more differentiated cultures, and resulting in progressive change in cell orientation and consequent loss of anisotropy. In contrast, the unrestricted cell contractility of myoblasts on planar (or convex) surfaces results in combined traction and push

forces promoting Rho-associated kinase (ROCK)-dependent cytoskeleton polymerization and lamin-dependent nuclear compression and deformation (Figure 7b).<sup>[37]</sup> This in turn promotes the nuclear translocation of active YAP, where it ultimately promotes *Pax7* expression and inhibits myogenesis (Figure 7b).<sup>[30,33b]</sup> Based on this model, milliscale convex surfaces could still be expected to promote myoblast anisotropy (following in-plane stress distribution) but ultimately limit or delay cell differentiation via mechanotransduction-associated pathways.

Inducing myoblast alignment and subsequent differentiation via surface patterning has a strong appeal compared with alternative methods such as mechanical, electric, magnetic, or biochemical stimulation,<sup>[3]</sup> being relatively accessible (i.e., affordable and easy to procure), versatile (i.e., effective on many adherent cell types), and reliant on “passive” cues (i.e., organization is driven by inherent cellular responses and not owing to external forces or active stimuli). However, reproducible nano- and microtopographies still rely on relatively complex surface fabrication techniques, making their large-scale production difficult. In contrast, milliscale curved surfaces, namely, those with concave geometries, are simpler to mass-produce and integrate in current cell and tissue culture systems. This availability increases considerably the potential of milliscale curved surfaces as preferential templates to biofabricate scaffold-free structured muscle tissues for therapeutic<sup>[41]</sup> and food applications.<sup>[5]</sup>

## 4. Conclusions

This study explored the role of milliscale surface curvature on the behavior of murine C2C12 myoblast migration, differentiation, and self-organization, illustrating the utility of such templates for promoting cell alignment and the formation of highly structured skeletal muscle tissues *in vitro*. These results open up the perspective of future studies in multiple areas, including cell biology, biotechnology, and tissue engineering. Investigating the impact of both convex and concave cues on myoblast mechanotransduction signaling will allow to test our proposed model and further clarify how these tissue-scale geometries affect muscle stem/progenitor cell behavior. Similarly, studying the impact of milliscale surface curvature on other adhesion-dependent cell types represents an obvious extension to the current work. Finally, milliscale curvature cues could help reduce the complexity and costs associated with mass production of structured tissues (e.g., skeletal muscle) for therapeutic and scientific applications, as well as for the nascent but rapidly growing field of cultured meat, where structure is particularly important for texture but difficult to reproduce using industrial processes.

## 5. Experimental Section

**Preparation of Curved Template Surfaces:** High-quality borosilicate glass tubes of variable internal diameter (3–50 mm; Cole-Palmer, UK) were custom-cut to produce halfpipe-shaped cell culture surfaces (Figure 1a,b) subsequently treated in a sonicating water bath for 15 min to remove any existing residues and sterilized by autoclaving at 121 °C for 20 min. Glass microscopy coverslips (Thermo Fisher Scientific, Waltham, MA) 22 × 18 mm in size were used as planar surface controls (Figure 1a). All culture surfaces were then coated with the cell-adhesive bioactive RGDS/ETTES peptide amphiphile.<sup>[42]</sup> Briefly, the peptide amphiphile solution ( $5 \times 10^{-4}$  M in deionized water) was applied onto the different glass surfaces ( $0.1 \text{ mL cm}^{-2}$ ) and left to dry overnight at room temperature inside a Class II biosafety cabinet and with rocking agitation to guarantee sterility and complete coating coverage (Figure 1c). Coating uniformity was evaluated by phase-contrast and fluorescence microscopy after incubation of both coated and noncoated surfaces with  $1 \times 10^{-3}$  M rhodamine B (Merck) for 1 h, followed by  $3 \times 15$  min washes with deionized water. Topographical analysis of the different curved and planar coated surfaces was performed by using an Easyscan 2-controlled AFM (Nanosurf, Switzerland) in static force mode and data processed for line-wise and tilt correction using the Scanning Probe Image Processor (SPIP) software package. Coatings were washed three times with sterile phosphate buffer saline (PBS) just prior to cell seeding.

**Cell Culture:** The murine C2C12 myoblast cell line was expanded in T25 flasks (Sarstedt, Germany) with 1:1 DMEM/F12 with glutamine and sodium pyruvate (Ref. 10565018; Thermo Fisher Scientific) supplemented with 10% heat-inactivated FBS (BioSera, France) and 1% penicillin/streptomycin (Thermo Fisher Scientific) (proliferation medium) at 37 °C and 5% CO<sub>2</sub> in a humidified cell culture incubator. Myoblasts were cultured until reaching 50–60% confluence, after which they were washed twice with PBS, detached using TrypLE (Thermo Fisher Scientific), and transferred onto new cell culture flasks at a low density (5000 cells  $\text{cm}^{-2}$ ). To test the effect of substrate curvature on myoblast behavior, C2C12 cells were seeded on the different surfaces (Figure 1a). Briefly, two UV-sterilized Parafilm M strips (Bemis, Neenah, WI) were custom-cut and gently applied 0.5 mm apart over the central region of each surface, along their long axis, using a digital stereo-microscope (Andonstar, China). Cells in suspension were then applied between the two strips and allowed to adhere to the unmasked surface for 30 min at 37 °C before removal of the masks. The resulting seeding comprised a narrow (500  $\mu\text{m}$ ) but well-defined line of closely packed C2C12 cells (100 000 cells

$\text{cm}^{-2}$ ) distributed along the surfaces' long axis (Figure 1d). Cells were then grown and allowed to migrate for 5 d within proliferation medium and subsequently differentiated in the following 5 d with DMEM/F12 supplemented with 2% heat-inactivated horse serum (Thermo Fisher Scientific) and 1% penicillin/streptomycin (differentiation medium). Media were replaced every day. Cells were used only until passage 5.

**Myoblast Migration Assay:** The outward/upward migration of C2C12 cells was monitored on both curved and planar surface types (Figure 1a) by time-lapse phase-contrast microscopy using an inverted Lumascope 500 (Etaluma, San Diego, CA). Briefly, microscopy images were taken every 5 min during the first 3 d in culture and binarized to better determine the position of individual cells in each image frame. The impact of surface geometry on cell distribution was evaluated from three independent fields of view. Cell migration rate ( $\mu\text{m min}^{-1}$ ) and tracks were determined from the position of 100 individual cells at the migration front, and tracing total covered distance as well as their pathways using the wrMTrack standard parameters (ImageJ v1.49). Data were expressed as the average  $\pm$  standard deviation (s.d.) from six independent experiments ( $n = 6$ ).

**Myoblast Adhesion, Proliferation, and Viability Assay:** The number of C2C12 cells attached and growing on curved and planar surfaces was evaluated at Day 1, 3, and 5 of culture using the Alamar Blue assay (Merck, Burlington, MA) as previously described.<sup>[42]</sup> Briefly, cells were incubated with 1:10 resazurin in growth medium for 2 h at 37 °C, with 50  $\mu\text{L}$  supernatant aliquots sampled and transferred in triplicate to flat-bottom 96-well plates (Greiner Bio-One, Germany) for fluorescence analysis at  $\lambda_{\text{em}} = 590$  nm using a Varioskan Lux microplate reader (Thermo Fisher Scientific). Cell number was calculated by standard curve interpolation using the fluorescence values of 1, 2, 5, 10, 20, and  $50 \times 10^4$  cells grown on normal tissue culture plates. Cell doubling time was calculated using Day 1 and 3 data to avoid the contact-inhibition effects of the crowded later-stage cultures, whereas cell numbers at Day 5 were used to evaluate total cell density in confluent monolayers in all tested conditions. To assess viability, C2C12 cells cultured for 5 d were incubated for 30 min with Calcein AM and propidium iodide dissolved in PBS at 1:10 000, followed by  $3 \times 5$  min washing with PBS, and imaged using an Axio Imager fluorescence microscope (Zeiss, Germany) at  $\lambda_{\text{em}} = 515$  and 620 nm to detect live and dead cells, respectively. Quantification of total viable cells was performed by analyzing ten different fields per sample. All experiments were performed six independent times ( $n = 6$ ).

**Cell Orientation Assay:** Cells growing on the various surfaces were imaged daily in three independent fields using a phase-contrast inverted microscope (Leica DM-IL LED) at 10 $\times$  magnification. Cell distribution and orientation were determined from phase-contrast microscopy images taken at Day 5 and 10 using the OrientationJ plugin for ImageJ v1.49. Specifically, images were analyzed using the direction and distribution functions (Gaussian gradient tensor  $\sigma = 1$  pixel; grid size = 50; scale = 2; coherency = 70), with cell orientation calculated between 0° and 180° (corresponding to at least 100 independent vectors per field of view, pooled in 1° angle bins), with 0° and 90° orientations being parallel to the long axis and arc axis, respectively. For tissues formed on planar templates, all binning combinations within an arbitrary parallel were considered. All experiments were performed six times, independently ( $n = 6$ ).

**Reverse-Transcription Quantitative Polymerase Chain Reaction:** Cells grown on the various surfaces for 5 or 10 d were harvested for RNA isolation using the standard Trizol extraction method, according to the manufacturer's method (Thermo Fisher Scientific). The quality of extracted RNA (ratio of absorbance at 260/280 nm within the 1.7–2.0 range) was verified using a NanoDrop 2000 spectrophotometer (Thermo Fisher Scientific). Synthesis of cDNA from isolated total RNA was performed by RT using the QuantiTect Reverse Transcription Kit (Qiagen, Germany) according to the manufacturer's instructions, in a TcPlus thermocycler (Techne, UK). RT-qPCR was performed using the Eco Real-Time PCR System (Illumina, San Diego, CA), with 40 $\times$  three-step cycle in a thermal profile of 10 s denaturation at 95 °C, 30 s annealing at 60 °C, and 15 s elongation at 72 °C. The relative expression of gene markers for undifferentiated cells (*Pax7* and *Abcg2*) as well as early-stage (*Myod1* and *Ache*) and late-stage differentiation gene markers (*Myh3* and *Myog*) was calculated by the comparative

**Table 1.** Specific primer pairs used to evaluate gene transcription by RT-qPCR.

Gene	Forward (5'–3')	Reverse (5'–3')
<i>Abcg2</i>	CAGATATCAATGGGATCATG	CATCTAGCAACGAAGACTTGC
<i>Ache</i>	CTGGGGTGC GGATCGGTGTACCCC	TCACAGGTCTGAGCAGCGTTCCTG
<i>Gapdh</i>	AGGTCGGTGTGAACGGATTG	TGTAGACCATGTAGTTGAGGTCA
<i>Myh3</i>	GATCCTCTCCTTTCCGACTTG	TCTGTACAGCTCAGAGGTGT
<i>Myod1</i>	TACAGTGGCGACTCAGATGC	GAGATGCGCTCCACTATGCT
<i>Myog</i>	CTACAGGCCTTGCTCAGCTC	ACGATGGACGTAAGGGAGTG
<i>Pax7</i>	GAAGAAGTCCCAGCACAGC	GCTACCAGTACAGCCAGTATG

threshold cycle (CT) (Eco Software v3.1, Illumina) and normalized to the expression of the *Gapdh* housekeeping gene (primer sequences indicated in **Table 1**), with data analyzed from four independent assays ( $n = 4$ ).

**Immunofluorescence Confocal Microscopy Analysis:** Cells grown on the various surfaces were fixed for 15 min at 4 °C with ice-cold methanol, incubated twice with PBS/0.1% Triton X-100 (Merck) wash solution for 5 min, as well as with blocking solution comprising 3% bovine serum albumin (First Link, UK) in wash solution for 1 h at room temperature. Cells were then incubated with rabbit anti-Pax7 (ab187339; Abcam, UK) and mouse anti-MyoD and anti-MHY (sc-377460 and sc-376157, respectively; Santa Cruz Biotechnology, Germany) diluted 1:200 in blocking solution for 2 h at room temperature, washed thrice for 5 min, and incubated with corresponding donkey anti-rabbit Alexa 594- or goat anti-mouse Alexa 488-conjugated secondary antibodies (R37119 and A11029, respectively; Thermo Fisher Scientific) and DAPI nuclear stain (Thermo Fisher Scientific) diluted 1:1:1000 in blocking solution for 1 h at room temperature. Cells were then washed, immersed in anti-fade medium comprising 1:1 PBS/glycerol with 2% (w/v) *n*-propyl-gallate (Merck), and imaged using an A1R Nikon confocal laser microscope (Nikon, Japan) with constant illumination and capture parameters. Microscopy images were analyzed using the NIS-Elements and ImageJ v1.49 software packages, with data evaluated from four independent assays ( $n = 4$ ).

**Statistical Analysis:** Data from all experiments were normalized to the corresponding control, analyzed a priori for homogeneity of variance, and presented as average values, with error bars representing the s.d. of the mean. Differences between groups were determined using one-way analysis of variance (ANOVA) followed by Bonferroni's multiple comparison *post hoc* test, using the GraphPad Prism (v6.07) software package. Significance between groups was established for  $p < 0.05$ , 0.01, and 0.001 (represented as \*, \*\*, and \*\*\*, respectively) and with a 95% confidence interval. For all assays, error bars represented the s.d. of the mean, analyzed a priori for homogeneity of variance.

## Supporting Information

Supporting Information is available from the Wiley Online Library or from the author.

## Acknowledgements

The authors thank New Harvest for the financial and scientific support. The authors thank Prof. Volker Straub, Newcastle University for kindly providing the cell lines used in this work. This work was supported by a New Harvest Research Fellowship (awarded to R.M.G.) and by the Biotechnology and Biological Sciences Research Council (BBSRC-UK).

## Conflict of Interest

The authors declare having no conflict of interest.

## Data Availability Statement

The data that support the findings of this study are available from the corresponding author upon reasonable request.

## Keywords

cell alignment, muscle differentiation, myoblasts, self-organization, surface curvature

Received: September 14, 2020

Revised: January 23, 2021

Published online:

- [1] J. M. Hernandez-Hernandez, E. G. Garcia-Gonzalez, C. E. Brun, M. A. Rudnicki, *Semin. Cell Dev. Biol.* **2017**, *72*, 10.
- [2] a) J. Chal, O. Pourquie, *Development* **2017**, *144*, 2104; b) V. Chaturvedi, D. E. Dye, B. F. Kinnear, T. H. van Kuppevelt, M. D. Grounds, D. R. Coombe, *PLoS One* **2015**, *10*, e0127675; c) J. Gingras, R. M. Rioux, D. Cuvelier, N. A. Geisse, J. W. Lichtman, G. M. Whitesides, L. Mahadevan, J. R. Sanes, *Biophys. J.* **2009**, *97*, 2771.
- [3] S. Ostrovidov, V. Hosseini, S. Ahadian, T. Fujie, S. P. Parthiban, M. Ramalingam, H. Bae, H. Kaji, A. Khademhosseini, *Tissue Eng., Part B* **2014**, *20*, 403.
- [4] S. Jana, S. K. Levengood, M. Zhang, *Adv. Mater.* **2016**, *28*, 10588.
- [5] T. Ben-Arye, S. Levenberg, *Front. Sustainable Food Syst.* **2019**, *3*, 46.
- [6] K. H. Nakayama, M. Shayan, N. F. Huang, *Adv. Healthcare Mater.* **2019**, *8*, 1801168.
- [7] a) C. G. Anene-Nzulu, K. Y. Peh, A. Fraiszudeen, Y. H. Kuan, S. H. Ng, Y. C. Toh, H. L. Leo, H. Yu, *Lab Chip* **2013**, *13*, 4124; b) A. Bettadapur, G. C. Suh, N. A. Geisse, E. R. Wang, C. Hua, H. A. Huber, A. A. Viscio, J. Y. Kim, J. B. Strickland, M. L. McCain, *Sci. Rep.* **2016**, *6*, 28855; c) M. T. Lam, S. Sim, X. Zhu, S. Takayama, *Biomaterials* **2006**, *27*, 4340; d) W. Y. Yeong, H. Yu, K. P. Lim, K. L. Ng, Y. C. Boey, V. S. Subbu, L. P. Tan, *Tissue Eng., Part C* **2010**, *16*, 1011.
- [8] S. Bansai, T. Morikura, H. Onoe, S. Miyata, *Micromachines* **2019**, *10*, 399.
- [9] M. Yeo, G. H. Kim, *Small* **2018**, *14*, 1803491.
- [10] G. H. Yang, J. Lee, G. Kim, *Biofabrication* **2019**, *11*, 025005.
- [11] I. M. Basurto, M. T. Mora, G. M. Gardner, G. J. Christ, S. R. Caliani, *bioRxiv* **2020**.
- [12] W. Li, Z. Yan, J. Ren, X. Qu, *Chem. Soc. Rev.* **2018**, *47*, 8639.
- [13] M. J. Dalby, *Int. J. Nanomed.* **2007**, *2*, 373.
- [14] D. Baptista, L. Teixeira, C. van Blitterswijk, S. Giselbrecht, R. Truckenmuller, *Trends Biotechnol.* **2019**, *37*, 838.
- [15] C. M. Nelson, R. P. Jean, J. L. Tan, W. F. Liu, N. J. Sniadecki, A. A. Spector, C. S. Chen, *Proc. Natl. Acad. Sci. USA* **2005**, *102*, 11594.
- [16] a) W. Du, J. Chen, H. Li, G. Zhao, G. Liu, W. Zhu, D. Wu, J. Chu, *J. Mater. Chem. B* **2016**, *4*, 3998; b) M. Rumpel, A. Woesz, J. W. Dunlop, J. T. van Dongen, P. Fratzl, *J. R. Soc., Interface* **2008**, *5*, 1173.
- [17] a) M. Werner, N. A. Kurniawan, G. Korus, C. V. C. Bouten, A. Petersen, *J. R. Soc., Interface* **2018**, *15*, 20180162; b) S. J. P. Callens, R. J. C. Uyttendaele, L. E. Fratila-Apachitei, A. A. Zadpoor, *Biomaterials* **2020**, *232*, 119739; c) S. J. Lee, S. Yang, *Biotechnol. J.* **2017**, *12*, 1700360; d) X. Lin, S. Romanazzo, K. Lin, C. Kelly, J. J. Gooding, I. Roohani, *Materialia* **2020**, *14*, 100870; e) T. Sun, Q. Shi, Q. Liang, Y. Yao, H. Wang, J. Sun, Q. Huang, T. Fukuda, *Lab Chip* **2020**, *20*, 3120; f) T. Yamashita, T. Nishina, I. Matsushita, R. Sudo, *Anal. Sci.* **2020**, *36*, 1015.

- [18] a) R. M. Gouveia, E. Koudouna, J. Jester, F. Figueiredo, C. J. Connon, *Adv. Biosyst.* **2017**, *1*, 1700135; b) M. Miotto, R. M. Gouveia, A. M. Ionescu, F. Figueiredo, I. W. Hamley, C. J. Connon, *Adv. Funct. Mater.* **2019**, *29*, 1807334.
- [19] a) X. He, Y. Jiang, *Phys. Biol.* **2017**, *14*, 035006; b) M. Pilia, T. Guda, S. M. Shiels, M. R. Appleford, *J. Biol. Eng.* **2013**, *7*, 23; c) M. Werner, S. B. Blanquer, S. P. Haimi, G. Korus, J. W. Dunlop, G. N. Duda, D. W. Grijpma, A. Petersen, *Adv. Sci.* **2017**, *4*, 1600347.
- [20] P. S. Zammit, F. Relaix, Y. Nagata, A. P. Ruiz, C. A. Collins, T. A. Partridge, J. R. Beauchamp, *J. Cell Sci.* **2006**, *119*, 1824.
- [21] L. Li, W. C. Xiong, L. Mei, *Annu. Rev. Physiol.* **2018**, *80*, 159.
- [22] R. M. Gouveia, E. Gonzalez-Andrades, J. C. Cardona, C. Gonzalez-Gallardo, A. M. Ionescu, I. Garzon, M. Alaminos, M. Gonzalez-Andrades, C. J. Connon, *Biomaterials* **2017**, *121*, 205.
- [23] S. Pina, V. P. Ribeiro, C. F. Marques, F. R. Maia, T. H. Silva, R. L. Reis, J. M. Oliveira, *Materials* **2019**, *12*, 1824.
- [24] E. W. Li, O. C. McKee-Muir, P. M. Gilbert, *Curr. Top. Dev. Biol.* **2018**, *126*, 125.
- [25] F. S. Tedesco, A. Dellavalle, J. Diaz-Manera, G. Messina, G. Cossu, *J. Clin. Invest.* **2010**, *120*, 11.
- [26] M. Werner, A. Petersen, N. A. Kurniawan, C. V. C. Bouten, *Adv. Biosyst.* **2019**, *3*, 1900080.
- [27] a) M. Beldjilali-Labro, A. G. Garcia, F. Farhat, F. Bedoui, J. F. Grosset, M. Dufresne, C. Legallais, *Materials* **2018**, *11*, 1116; b) S. Jana, M. Zhang, *J. Mater. Chem. B* **2013**, *1*, 2575; c) N. Narayanan, C. Jiang, C. Wang, G. Uzunalli, N. Whittern, D. Chen, O. G. Jones, S. Kuang, M. Deng, *Front. Bioeng. Biotechnol.* **2020**, *8*, 203.
- [28] Y. J. Choi, S. J. Park, H. G. Yi, H. Lee, D. S. Kim, D. W. Cho, *J. Mater. Chem. B* **2018**, *6*, 5530.
- [29] M. S. Grigola, C. L. Dyck, D. S. Babacan, D. N. Joaquin, K. J. Hsia, *Biotechnol. Bioeng.* **2014**, *111*, 1617.
- [30] M. Fischer, P. Rikeit, P. Knaus, C. Coirault, *Front. Physiol.* **2016**, *7*, 41.
- [31] V. Chaturvedi, D. Naskar, B. F. Kinnear, E. Grenik, D. E. Dye, M. D. Grounds, S. C. Kundu, D. R. Coombe, *J. Tissue Eng. Regen. Med.* **2017**, *11*, 3178.
- [32] S. Romanazzo, G. Forte, M. Ebara, K. Uto, S. Pagliari, T. Aoyagi, E. Traversa, A. Taniguchi, *Sci. Technol. Adv. Mater.* **2012**, *13*, 064211.
- [33] a) T. H. Chen, C. Y. Chen, H. C. Wen, C. C. Chang, H. D. Wang, C. P. Chuu, C. H. Chang, *FASEB J.* **2017**, *31*, 2963; b) R. N. Judson, A. M. Tremblay, P. Knopp, R. B. White, R. Urcia, C. De Bari, P. S. Zammit, F. D. Camargo, H. Wackerhage, *J. Cell Sci.* **2012**, *125*, 6009; c) K. I. Watt, R. Judson, P. Medlow, K. Reid, T. B. Kurth, J. G. Burniston, A. Ratkevicius, C. De Bari, H. Wackerhage, *Biochem. Biophys. Res. Commun.* **2010**, *393*, 619.
- [34] F. Trens, F. Lucien, V. Couture, T. Sollrard, G. Drouin, A. J. Rouleau, M. Grandbois, G. Lacraz, G. Grenier, *Skeletal Muscle* **2015**, *5*, 5.
- [35] S. Ehrig, B. Schamberger, C. M. Bidan, A. West, C. Jacobi, K. Lam, P. Kollmannsberger, A. Petersen, P. Tomancak, K. Kommareddy, F. D. Fischer, P. Fratzl, J. W. C. Dunlop, *Sci. Adv.* **2019**, *5*, eaav9394.
- [36] A. B. C. Buskermolen, H. Suresh, S. S. Shishvan, A. Vigliotti, A. DeSimone, N. A. Kurniawan, C. V. C. Bouten, V. S. Deshpande, *Biophys. J.* **2019**, *116*, 1994.
- [37] M. Werner, N. A. Kurniawan, C. V. C. Bouten, *Materials* **2020**, *13*, 963.
- [38] C. Bruyere, M. Versaevel, D. Mohammed, L. Alaimo, M. Luciano, E. Vercruyssen, S. Gabriele, *Sci. Rep.* **2019**, *9*, 15565.
- [39] B. Ladoux, R. M. Mege, *Nat. Rev. Mol. Cell Biol.* **2017**, *18*, 743.
- [40] C. Liu, J. Xu, S. He, W. Zhang, H. Li, B. Huo, B. Ji, *J. Mech. Behav. Biomed. Mater.* **2018**, *88*, 330.
- [41] M. D. Grounds, *Clin. Exp. Pharmacol. Physiol.* **2018**, *45*, 390.
- [42] R. M. Gouveia, V. Castelletto, S. G. Alcock, I. W. Hamley, C. J. Connon, *J. Mater. Chem. B* **2013**, *1*, 6157.